Dynamic Response of Wigner Crystals

Lili Zhao,[1] Wenlu Lin,[1] Yoon Jang Chung,[2] Adbhut Gupta,[2] Kirk W. Baldwin,[2]
Loren N. Pfeiffer,[2] and Yang Liu[1,*]
[1]International Center for Quantum Materials, Peking University, Haidian, Beijing 100871, China
[2]Department of Electrical Engineering, Princeton University, Princeton, New Jersey 08544, USA

(Received 28 December 2022; accepted 26 May 2023; published 15 June 2023)

The Wigner crystal, an ordered array of electrons, is one of the very first proposed many-body phases stabilized by the electron-electron interaction. We examine this quantum phase with simultaneous capacitance and conductance measurements, and observe a large capacitive response while the conductance vanishes. We study one sample with four devices whose length scale is comparable with the crystal's correlation length, and deduce the crystal's elastic modulus, permittivity, pinning strength, etc. Such a systematic quantitative investigation of all properties on a single sample has a great promise to advance the study of Wigner crystals.

DOI: 10.1103/PhysRevLett.130.246401

Interacting two-dimensional electron systems (2DESs) subjected to large perpendicular magnetic fields (B) exhibit a plethora of exotic states [1]. The Wigner crystal (WC) [2] develops at very small landau level filling factor [3–25]. This electron solid is pinned by the ubiquitous residual disorder and manifests as an insulating phase in dc transport [3–11], and the electrons' collective motion is evidenced by a resonance in ac transport [12–20]. A series of experiments have been applied to investigate this solid, such as the nonlinear $I-V$ [4,16], the noise spectrum [5], the screening efficiency [22], the melting [22–24], the nuclear magnetic resonance [25], the optics [26,27], and so on.

Capacitance measurements have revealed a series of quantum phenomena [22,28–39]. In this Letter, we examine the WC formed at $\nu \lesssim 1/5$ using high-precision capacitance measurement [40,41]. We find a large capacitance at low frequency f while the conductance is almost zero. This phenomenon is an evidence that the synchronous vibration of electrons induces a polarization current. When we increase f, our high-precision measurement captures the fine structure of resonance. Our systematic, quantitative results provide an in-depth insight of this murky quantum phase.

Our sample is a 2×2 mm square piece from a GaAs/AlGaAs wafer consisting an ultraclean low-density 2DES confined in a 70-nm-wide GaAs quantum well at $h \simeq 960$ nm below the surface. The as-grown density n is 4.4×10^{10} cm^{-2} and mobility at 300 mK is 17×10^6 cm$^2/(\mathrm{V}\cdot\mathrm{s})$. The sample consists multiple individual devices. Each device has a pair of Corbino-like front gates, G1 and G2, whose outer and inner radius are r_1 and r_2, respectively; see the inset of Fig. 1(a). We study four devices with $r_1 = 60$ μm and $r_2 = 60$, 80, 100, and 140 μm, respectively [42]. We measure the capacitance C (and conductance G) between two gates using a cryogenic bridge; see the inset of Fig. 1(a) [40,41]. C and G can be calculated from the in-phase and out-phase components of the bridge output V_{out}, respectively [43].

Figure 1(a) shows the C and G measured from the $r_1 = r_2 = 60$ μm device. C decreases dramatically with B. This is because the ultrahigh mobility 2DES conductivity $\sigma = ne^2\tau/m^* \cdot (1+\omega_c^2\tau^2)^{-1}$ vanishes when $\omega_c\tau \gg 1$ at $B \gtrsim 0.1$ T, where m^*, ω_c, and τ are the effective mass, cyclotron frequency, and transport scattering time of the electrons, respectively. At high field, only a narrow region $\propto \sqrt{\sigma}$ around the gate boundary can be charged. A careful study shows that $C \propto G^{3/2}$ is expected when the current is carried by "transporting electrons" [41]. The C and G are finite at $\nu = 1/2$ and $1/4$ where the 2DES forms compressible composite fermion Fermi sea. When ν is an integer or a certain fraction such as $1/3$ and $1/5$, the 2DES forms incompressible quantum Hall liquids so that both C and G vanish [44].

The $C \propto G^{3/2}$ relation for current carried by transporting electrons in Fig. 1(b), discontinues when the WC forms at very low filling factors $\nu \lesssim 1/5$ in the blue shaded regions of Fig. 1(a). The vanishing G suggests that the electrons are immovable. Surprisingly, the C becomes much larger than its value at $\nu = 1/2$ and $1/4$ (~0.2 pF vs ~0.02 pF), evidencing that the WC is more effective in transferring charges than the conducting Fermi sea. The phase transition between WC and liquid states is clearly evidenced by spikes in G and sharp raises in C [marked by solid circles in Fig. 1(a)]. A developing minimum is seen in G at $1/5 < \nu < 2/9$ (marked by the up arrow) when C has a peak. This G minimum develops toward zero and the C peak saturates when the solid phase is stronger [see black traces in Fig. 3(a)]. This is consistent with the reentrant insulating phase [3–5,16,19].

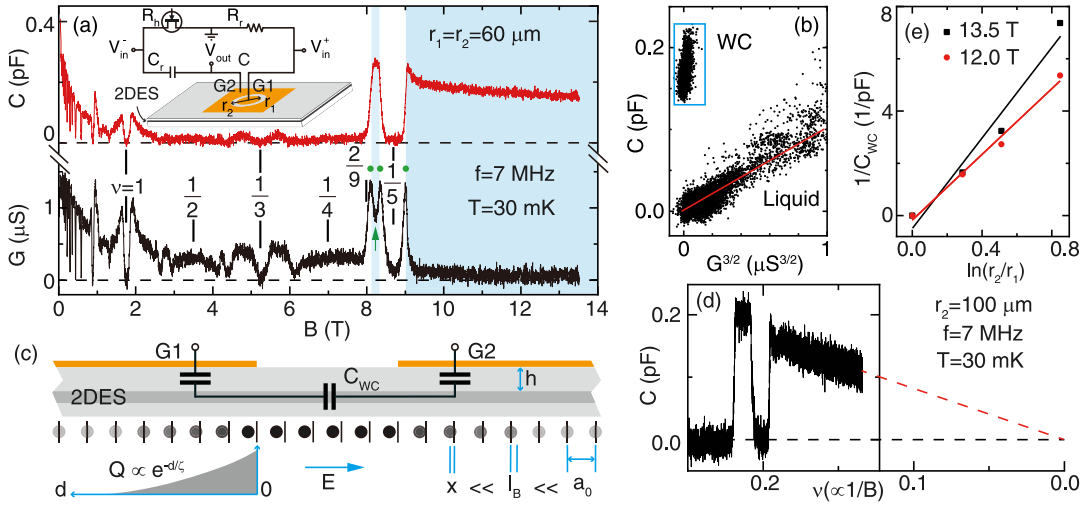

FIG. 1. (a) C and G measured from the $r_1 = r_2 = 60$ μm device with $f \simeq 7$ MHz at 30 mK. The horizontal dashed lines represent the zeros of C or G. The blue shaded regions mark the presence of WC. Inset is the cartoon of device and bridge with four arms: R_h, R_r, C_r, and C. (b) The relation plot between C and G data in panel (a). Transporting current dominates at $B < 8$ T where $C \propto G^{3/2}$, indicated by the red solid line. When the WC forms, $C \sim 0.2$ pF and G is about zero (the blue box). (c) The schematic model describing the collective motion of electrons in the pinned WC. h is the 2DES depth. The equally spaced (by the lattice constant a_0) vertical bars represent the equilibrium position of electrons. The gray-scaled solid circles represent the electron position at finite external electric field $\boldsymbol{E}$. The darker gray corresponds to larger electron displacement $\boldsymbol{x}$. The radius of individual electron is about the magnetic length l_B. The accumulated charge Q is proportional to $\nabla \cdot \boldsymbol{x}$, and decays exponentially as a function of the distance d from the gate boundary. ζ is the decay length. C_{WC} is the effective capacitance of WC in the ungated region between two gates. (d) C vs ν of the $r_2 = 100$ μm device. The black dashed line is the zero of C. The red dashed line is the linear extension of data, showing that $C = 0$ at the extreme quantum limit $\nu = 0$. (e) $1/C_{\mathrm{WC}}$ vs $\ln(r_2/r_1)$ at two different magnetic fields.

It is important to mention that the 2DES in our devices is effectively "isolated": no electrons move in or out of the device region, and we are merely transferring charges between two gates within one quantum phase. Similar to the dielectric materials that also have no transporting electrons, the collective motion of all electrons can generate "polarization charges" and corresponding polarization current in response to the in-plane component of applied electric field. An infinitesimally small but ubiquitous disorder pins the WC so that electrons can only be driven out of their equilibrium lattice site by a small displacement $\boldsymbol{x}$, as shown in Fig. 1(c). During the experiments, we use excitation $V_{\mathrm{in}} \simeq 0.1$ $\mathrm{mV_{rms}}$ and the measured capacitance is ~0.13 pF at 13.5 T. The polarization charge accumulated under the inner gate is $Q = CV_{\mathrm{in}} \sim 100e$. The corresponding electron displacement at the boundary of the inner gate, $|\boldsymbol{x}(r_1)| \simeq Q/(2\pi r_1 ne) \sim 0.6$ nm, is much smaller than the magnetic length $l_B = \sqrt{\hbar/eB} \sim 7$ nm, substantiating our assumption that the electrons vibrate diminutively around their equilibrium lattice sites.

An ideal, disorder-free WC is effectively a perfect dielectric with infinite permittivity, so that the device capacitance should be close to its zero-field value $C_0 \sim 1$ pF, which is consistent with the device geometry, $\epsilon_0 \epsilon_{\mathrm{GaAs}} \pi r_1^2/h \simeq 1.3$ pF, where $\epsilon_{\mathrm{GaAs}} \approx 12.8$ is the relative permittivity of GaAs. However, the measured $C \sim 0.13$ pF in the WC regime is much smaller than C_0. This discrepancy is likely caused by the frictionlike disorder that poses a pinning force $\simeq -\beta \boldsymbol{x}$ on the electrons. When $\boldsymbol{x}$ is nonuniform and $\mathcal{J}(\boldsymbol{x})$ is finite, the electron-electron interaction generates a restoring force $\simeq -a_0 \mu_{ij} \mathcal{J}(\boldsymbol{x})$, where μ_{ij}, $a_0 [= (2/\sqrt{3}n)^{1/2} \simeq 52$ nm], and $\mathcal{J}(\boldsymbol{x})$ are the elastic tensor, WC lattice constant, and the Jacobi matrix of $\boldsymbol{x}$, respectively. At the low frequency limit, the WC is always at equilibrium and all forces are balanced, $e\boldsymbol{E} - a_0 \mu_{ij} \mathcal{J}(\boldsymbol{x}) - \beta \boldsymbol{x} = 0$. $\boldsymbol{E}$ is the total parallel electric field on the WC.

$\boldsymbol{E}$ is approximately zero under the metal gates since the gate-to-2DES distance h is small. Therefore, $\boldsymbol{x}$ decreases exponentially when the distance from the gate boundary d increases, $\boldsymbol{x} \propto \exp(-d/\zeta)$, where $\zeta = \mu a_0/\beta$ is the decay length. Deep inside the gates, electrons feel neither parallel electric field nor net pressure from nearby electrons, so that their displacement $\boldsymbol{x}$ remains approximately zero. This region does not contribute to the capacitive response, and the effective gate area reduces to about $2\pi r_1 \zeta$ and $2\pi r_2 \zeta$ at the inner and outer gate, respectively. Because $r_1 = r_2 = 60$ μm in Fig. 1(a), the experimentally measured $C \approx \epsilon_0 \epsilon_{\mathrm{GaAs}}/h \cdot 2\pi r_1 \zeta/2 \simeq 0.13$ pF at 13.5 T corresponds to a decay length $\zeta \simeq 5.9$ μm. Interestingly, our result shows a linear dependence $C \propto 1/B$ in Fig. 1(d), suggesting that $\beta \propto l_B^{-2}$ if we assume μ_{ij} is independent on B. Especially, the pinning becomes infinitely strong, i.e., $\beta \to \infty$, at the extreme quantum limit $l_B \to 0$.

The permittivity of a disorder-pinned WC is no longer infinitely large, since a nonzero electric field $\boldsymbol{E}$ is necessary to sustain a finite $\boldsymbol{x}$. $\boldsymbol{x}$ is a constant in the ring area between the two gates, so that $e\boldsymbol{E} = \beta\boldsymbol{x}$. $\boldsymbol{E}$ can be modeled as a serial capacitance $C_{\rm WC} \approx 2\pi n e^2/\beta \cdot [\ln(r_2/r_1)]^{-1}$. We then measure different devices with $r_2 = 60$, 80, 100, and 140 μm, and calculate $C_{\rm WC}$ through $C_{\rm WC}^{-1} = C^{-1} - (r_1 + r_2)/2r_2 \cdot C_{r_1=r_2}^{-1}$; see Fig. 1(e). By fitting $C_{\rm WC}^{-1} \propto \ln(r_2/r_1)$, we estimate the pinning strength β to be about 6.1×10^{-10} and 4.4×10^{-10} N/m at $B = 13.5$ and 12 T, respectively. Finally, assuming $\mu_{ij} \approx \mu \cdot \delta_{ij}$, we can estimate the WC elastic modulus $\mu \approx \beta \cdot \zeta/a_0$. For example, μ is about 6.9×10^{-8} N/m at 13.5 T, consistent with the theoretical predicted shear modulus of classical WC, $\mu_{\rm cl} = 0.245 e^2 n^{3/2}/4\pi\epsilon_0\epsilon_{\rm GaAs} \simeq 3.8 \times 10^{-8}$ N/m [45]. Alternatively, $C_{\rm WC}$ can be modeled as a cylinder capacitor whose height equals the effective thickness of the 2DES, $Z_0 \approx 45$ nm from the self-consistent solution of energy bands. The WC permittivity is $\epsilon_{\rm WC} = [2\pi\epsilon_0 Z_0 \partial(C_{\rm WC}^{-1})/\partial \ln(r_2/r_1)]^{-1}$. At 13.5 T, $\epsilon_{\rm WC} \simeq 4.6 \times 10^4$ consistent with previous reported value in Ref. [21].

Figure 2 reveals an intriguing temperature-induced solid-liquid phase transition when the WC melts. Figure 2(a) shows C and G taken from the $r_2 = 80$ μm device at various temperatures. At a certain temperature, e.g., $T \approx 110$ mK, $C \sim 0.2$ pF when WC forms at $\nu \lesssim 0.16$ and vanishes when 2DES is a liquid phase at $\nu \gtrsim 0.19$. G has a peak at $\nu \simeq 0.175$ when C vs ν has the maximal negative slope, and it is small when the 2DES is either a WC or a liquid [46]. At $T \gtrsim 200$ mK, both C and G are close to zero. In Fig. 2(b), we summarized C and G as a function of T at two filling factors to better illustrate this transition. At $\nu \simeq 0.14$, for example, C is large and G is small at $T \lesssim 100$ mK when the WC is stable [47], while both of them become small at $T \gtrsim 200$ mK at liquid phase. The G has a peak at a critical temperature T_C, marked by the red arrows, around which the precipitous decrease of C happens. Alternatively, T_C at a certain filling factor can be defined as the temperature when the G has a peak [black arrow in Fig. 2(a)] with ν. We summarize T_C obtained using two equivalent procedures in the Fig. 2(b) inset with corresponding red and black symbols. T_C has a linear dependence on ν and two intercepts: $T_C \simeq 340$ mK at the extreme quantum limit $\nu = 0$, $\nu \simeq 1/4$ at $T_C = 0$ mK.

The Fig. 2(b) evolution can be qualitatively understood by the coexistence of transport and polarization currents at the solid-liquid transition. The large C reduces to almost zero when the transport current dominates over the polarization current. G is a measure of the 2DES's capacity to absorb and dissipate power. It is negligible if either of these two currents dominates, since the polarization current is dissipation-less and the dissipating transport current is difficult to excite. G becomes large when these two currents coexist nip and tuck at intermediate T when the excited polarization charge can be just dissipated by the transport current.

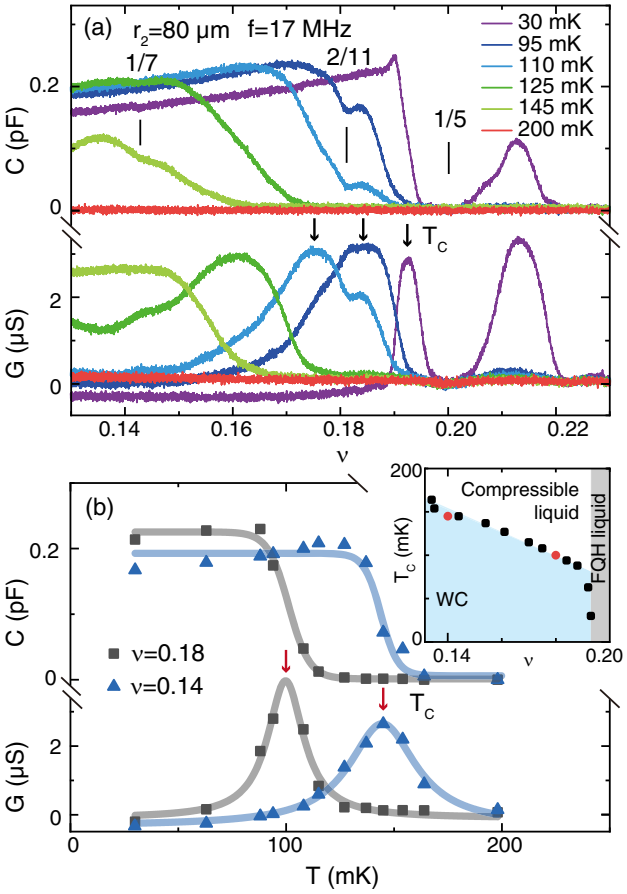

FIG. 2. (a) C and G vs ν measured at various temperatures from the $r_2 = 80$ μm device with $f \simeq 17$ MHz. (b) Summarized C and G vs T at $\nu = 0.14$ and 0.18 from the panel (a) data. Critical temperature T_c at certain ν is defined either as the temperature when G has a peak at ν in panel (a) or as the temperature when G vs T trace reaches maximum in panel (b), marked by the black and red arrows. The panel (b) inset summarizes the T_c using the two equivalent definitions by black and red points. The diagram can be separated into three different regions: the WC, the fractional quantum Hall (FQH) liquid, and the compressible liquid.

The WC exhibits a resonance when we increase f. In Fig. 3(a), the C and G measured from the $r_2 = 100$ μm device using different f change enormously when the WC presents (blue shaded region). G is almost zero and C is large at $f \simeq 7$ MHz, and G becomes finite and C becomes even larger at $f \simeq 23$ MHz. At $f \simeq 27$ MHz, G reaches its maximum and C drops to about zero. Further increasing f, G gradually declines while C first becomes negative and then gradually approaches zero. The summarized C and G vs f at two fillings in Fig. 3(b), resembles a resonance frequency $f_r \simeq 26$ MHz (when $C = 0$). This f_r is smaller than previous reports [18,19], possibly because our sample disorder is much lower. Figure 3(c) studies this resonance

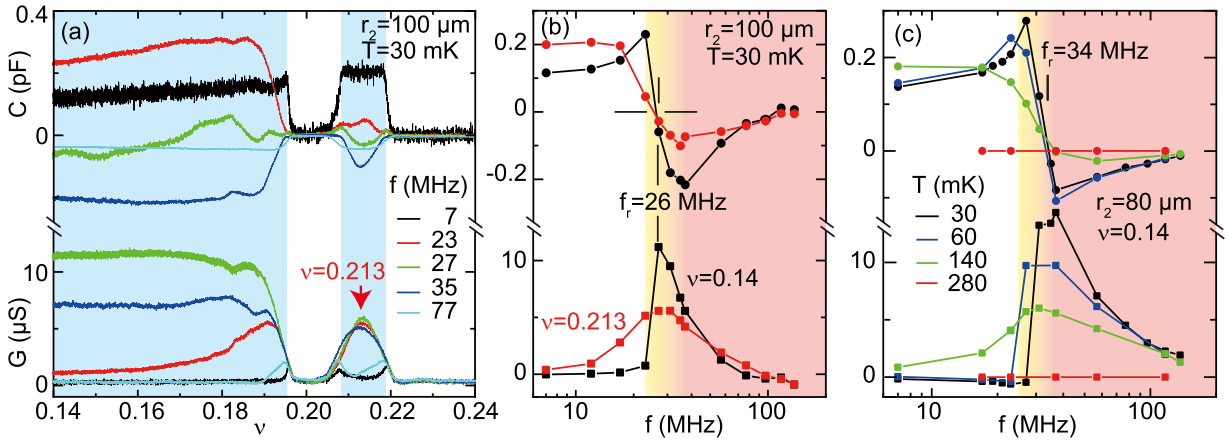

FIG. 3. (a) C and G vs ν taken from the $r_2 = 100$ μm device using different f. C and G change violently with f in the blue region where the WC appears. (b) C and G vs f extracted from the panel (a) trace at $\nu = 0.14$ and 0.213. f_r is about 26 MHz, defined as the frequency when C changes its sign. (c) C and G vs f at $\nu = 0.14$ and different temperatures, taken from the $r_2 = 80$ μm device. The resonance disappears at $T \simeq 280$ mK when C and G remain nearly zero.

at different temperatures. The data are taken from the $r_2 \simeq 80$ μm device with $f_r \simeq 34$ MHz [48]. The abrupt change of C near f_r becomes gradual and the G peak flattens at higher temperatures. Both C and G become flat zero at $T \gtrsim 280$ mK. It is noteworthy that, as long as a resonance is seen, f_r is nearly independent on the filling factor [Fig. 3(b)] [43] and temperatures [Fig. 3(c)]. This is consistent with experimental study using surface acoustic wave [24].

The resonance of WC is usually explained by the pinning mode [18,45]. f_r is related to the mean free path $L_T = (2\pi\mu_{cl}/neBf_r)^{1/2}$ of the transverse phonon. $f_r = 26$ MHz corresponds to $L_T \simeq 3.2$ μm, very similar to $\zeta \simeq 5.9$ μm in our Fig. 1(c) discussion. This is justifiable because both L_T and ζ describe the length scale within which the collective motion of WC is damped or scattered by the random pinning potential.

Before ending the discussion, we would like to highlight a puzzling resonance structure. G has a regular-shaped resonance peak, i.e., G decreases gradually on both sides of f_r when either the WC is weak [$\nu \simeq 0.213$ in Fig. 3(b)] or the temperature is high [$T \simeq 140$ mK in Fig. 3(c)]. Surprisingly, the resonance peak becomes quite peculiar when the WC is strong at $\nu \simeq 0.14$ and $T \simeq 30$ mK. G gradually decreases from its peak on the high frequency side $f > f_r$, while it vanishes instantly at $f < f_r$, resulting in a "half-dome" G vs f trace. Meanwhile, the C increases by ~2 times and then abruptly changes to negative at f_r. This anomalous half-dome feature is seen in all of our devices as long as the WC is strong and temperature is sufficiently low. The sharp raise of G at $f < f_r$ suggests a threshold frequency for exciting WC's dissipative phonon mode. Meanwhile, the slow decay of G at $f > f_r$ might be explained either by the reduced phonon heating effect, or the possible melting of WC. We wish future studies can provide more insights.

In conclusion, we investigate the dynamic response of WC by simultaneously measuring its capacitance and conductance. From the quantitative results, we can deduce the WC's physical properties such as elastic modulus, permittivity, pinning strength, etc., and discover a puzzling half-dome feature of the resonance. Our results provide new insight on WC's dynamics. Such a systematic study of all properties on one single sample has a great promise to advance the understanding of WC physics.

We acknowledge support by the National Natural Science Foundation of China (Grants No. 92065104 and No. 12074010) and the National Basic Research Program of China (Grant No. 2019YFA0308403) for sample fabrication and measurement. This research is funded in part by the Gordon and Betty Moore Foundation's EPiQS Initiative, Grant No. GBMF9615 to L. N. P., and by the National Science Foundation MRSEC Grant No. DMR 2011750 to Princeton University. We thank L. W. Engel, Bo Yang, and Xi Lin for valuable discussion.

*Corresponding author.
liuyang02@pku.edu.cn

[1] J. K. Jain, *Composite Fermions* (Cambridge University Press, Cambridge, UK, 2007).
[2] E. Wigner, Phys. Rev. **46**, 1002 (1934).
[3] H. W. Jiang, R. L. Willett, H. L. Stormer, D. C. Tsui, L. N. Pfeiffer, and K. W. West, Phys. Rev. Lett. **65**, 633 (1990).
[4] V. J. Goldman, M. Santos, M. Shayegan, and J. E. Cunningham, Phys. Rev. Lett. **65**, 2189 (1990).
[5] Y. P. Li, T. Sajoto, L. W. Engel, D. C. Tsui, and M. Shayegan, Phys. Rev. Lett. **67**, 1630 (1991).
[6] M. B. Santos, Y. W. Suen, M. Shayegan, Y. P. Li, L. W. Engel, and D. C. Tsui, Phys. Rev. Lett. **68**, 1188 (1992).
[7] T. Sajoto, Y. P. Li, L. W. Engel, D. C. Tsui, and M. Shayegan, Phys. Rev. Lett. **70**, 2321 (1993).

[8] W. Pan, H. L. Stormer, D. C. Tsui, L. N. Pfeiffer, K. W. Baldwin, and K. W. West, Phys. Rev. Lett. **88**, 176802 (2002).

[9] D. Maryenko, A. McCollam, J. Falson, Y. Kozuka, J. Bruin, U. Zeitler, and M. Kawasaki, Nat. Commun. **9**, 4356 (2018).

[10] M. S. Hossain, M. K. Ma, K. A. V. Rosales, Y. J. Chung, L. N. Pfeiffer, K. W. West, K. W. Baldwin, and M. Shayegan, Proc. Natl. Acad. Sci. U.S.A. **117**, 32244 (2020).

[11] Y. J. Chung, D. Graf, L. W. Engel, K. A. Villegas Rosales, P. T. Madathil, K. W. Baldwin, K. W. West, L. N. Pfeiffer, and M. Shayegan, Phys. Rev. Lett. **128**, 026802 (2022).

[12] Y. Lozovik and V. Yudson, JETP Lett. **22**, 11 (1975), http://jetpletters.ru/ps/1478/article_23247.shtml.

[13] P. K. Lam and S. M. Girvin, Phys. Rev. B **30**, 473 (1984).

[14] D. Levesque, J. J. Weis, and A. H. MacDonald, Phys. Rev. B **30**, 1056 (1984).

[15] E. Y. Andrei, G. Deville, D. C. Glattli, F. I. B. Williams, E. Paris, and B. Etienne, Phys. Rev. Lett. **60**, 2765 (1988).

[16] F. I. B. Williams, P. A. Wright, R. G. Clark, E. Y. Andrei, G. Deville, D. C. Glattli, O. Probst, B. Etienne, C. Dorin, C. T. Foxon, and J. J. Harris, Phys. Rev. Lett. **66**, 3285 (1991).

[17] C.-C. Li, L. W. Engel, D. Shahar, D. C. Tsui, and M. Shayegan, Phys. Rev. Lett. **79**, 1353 (1997).

[18] P. D. Ye, L. W. Engel, D. C. Tsui, R. M. Lewis, L. N. Pfeiffer, and K. West, Phys. Rev. Lett. **89**, 176802 (2002).

[19] Y. P. Chen, R. M. Lewis, L. W. Engel, D. C. Tsui, P. D. Ye, Z. H. Wang, L. N. Pfeiffer, and K. W. West, Phys. Rev. Lett. **93**, 206805 (2004).

[20] J. Jang, B. M. Hunt, L. N. Pfeiffer, K. W. West, and R. C. Ashoori, Nat. Phys. **13**, 340 (2017).

[21] Y. Li, D. Tsui, T. Sajoto, L. Engel, M. Santos, and M. Shayegan, Solid State Commun. **95**, 619 (1995).

[22] H. Deng, L. N. Pfeiffer, K. W. West, K. W. Baldwin, L. W. Engel, and M. Shayegan, Phys. Rev. Lett. **122**, 116601 (2019).

[23] Y. P. Chen, G. Sambandamurthy, Z. H. Wang, R. M. Lewis, L. W. Engel, D. C. Tsui, P. D. Ye, L. N. Pfeiffer, and K. W. West, Nat. Phys. **2**, 452 (2006).

[24] I. L. Drichko, I. Y. Smirnov, A. V. Suslov, Y. M. Galperin, L. N. Pfeiffer, and K. W. West, Phys. Rev. B **94**, 075420 (2016).

[25] L. Tiemann, T. D. Rhone, N. Shibata, and K. Muraki, Nat. Phys. **10**, 648 (2014).

[26] Y. Zhou, J. Sung, E. Brutschea, I. Esterlis, Y. Wang, G. Scuri, R. J. Gelly, H. Heo, T. Taniguchi, K. Watanabe, G. Zaránd, M. D. Lukin, P. Kim, E. Demler, and H. Park, Nature (London) **595**, 48 (2021).

[27] T. Smoleński, P. E. Dolgirev, C. Kuhlenkamp, A. Popert, Y. Shimazaki, P. Back, X. Lu, M. Kroner, K. Watanabe, T. Taniguchi, I. Esterlis, E. Demler, and A. Imamoğlu, Nature (London) **595**, 53 (2021).

[28] V. Mosser, D. Weiss, K. Klitzing, K. Ploog, and G. Weimann, Solid State Commun. **58**, 5 (1986).

[29] R. C. Ashoori, H. L. Stormer, J. S. Weiner, L. N. Pfeiffer, S. J. Pearton, K. W. Baldwin, and K. W. West, Phys. Rev. Lett. **68**, 3088 (1992).

[30] T. P. Smith, W. I. Wang, and P. J. Stiles, Phys. Rev. B **34**, 2995 (1986).

[31] M. J. Yang, C. H. Yang, B. R. Bennett, and B. V. Shanabrook, Phys. Rev. Lett. **78**, 4613 (1997).

[32] J. P. Eisenstein, L. N. Pfeiffer, and K. W. West, Phys. Rev. B **50**, 1760 (1994).

[33] A. A. Zibrov, C. Kometter, H. Zhou, E. M. Spanton, T. Taniguchi, K. Watanabe, M. P. Zaletel, and A. F. Young, Nature (London) **549**, 360 (2017).

[34] H. Irie, T. Akiho, and K. Muraki, Appl. Phys. Express **12**, 063004 (2019).

[35] J. P. Eisenstein, L. N. Pfeiffer, and K. W. West, Phys. Rev. Lett. **68**, 674 (1992).

[36] J. Jo, E. A. Garcia, K. M. Abkemeier, M. B. Santos, and M. Shayegan, Phys. Rev. B **47**, 4056 (1993).

[37] L. Li, C. Richter, S. Paetel, T. Kopp, J. Mannhart, and R. C. Ashoori, Science **332**, 825 (2011).

[38] A. A. Zibrov, P. Rao, C. Kometter, E. M. Spanton, J. I. A. Li, C. R. Dean, T. Taniguchi, K. Watanabe, M. Serbyn, and A. F. Young, Phys. Rev. Lett. **121**, 167601 (2018).

[39] S. L. Tomarken, Y. Cao, A. Demir, K. Watanabe, T. Taniguchi, P. Jarillo-Herrero, and R. C. Ashoori, Phys. Rev. Lett. **123**, 046601 (2019).

[40] L. Zhao, W. Lin, X. Fan, Y. Song, H. Lu, and Y. Liu, Rev. Sci. Instrum. **93**, 053910 (2022).

[41] L. Zhao, W. Lin, Y. J. Chung, K. W. Baldwin, L. N. Pfeiffer, and Y. Liu, Chin. Phys. Lett. **39**, 097301 (2022).

[42] We deposit a ~20 nm Al_2O_3 layer between two gates to avoid the shorting between two gates when $r_2 = r_1 = 60$ μm. Detailed fabrication steps are in the Supplemental Material [43].

[43] See Supplemental Material at http://link.aps.org/supplemental/10.1103/PhysRevLett.130.246401 for more information.

[44] The zero of C and G can be defined either by extrapolating their field dependence to $B = \infty$, or by their values at strong quantum hall states such as $\nu = 1$. These two approaches are consistent with each other and the dash lines in Fig. 1(a) represent the deduced zero.

[45] M. M. Fogler and D. A. Huse, Phys. Rev. B **62**, 7553 (2000).

[46] We observe developing minimum at $\nu = 1/7, 2/11$ during the solid-liquid phase transition, signaling that the fractional quantum Hall state emerges [8,11].

[47] C vs T has a slightly positive slope in the WC region, possibly due to the softening of disorder pinning.

[48] f_r has no obvious dependence with device geometry, which is about 35, 34, 26, and 29 MHz for devices with $r_2 = 60$, 80, 100, 140 μm, respectively.